UNIABUJA Journal of Engineering and Technology

https://ujet.uniabuja.edu.ng/

ISSN: 2714-3236 (Online); 2714-3228 (Print)

Volume 3, Issue 2, 2026; 395-402

Stochastic Deflection of Axially Loaded Timoshenko Beam-Columns under Random Non-Stationary Dynamic Impact across Different End Conditions for Bridge Piers

Franklyn O. NNEBE[1], Emmanuel E. NDUBUBA[2], Kamoru SALAM[3]

[1]*Department of Civil Engineering, Nile University, Abuja, Nigeria*
[2]*Department of Civil Engineering, University of Abuja, Abuja, Nigeria*
[3]*Department of Chemical Engineering, University of Abuja, Abuja, Nigeria*

[1]*nnebe.Franklyn@nileuniversity.edu.ng*, [2]*emmanuel.ndububa@uniabuja.edu.ng*, [3]*kamoru.salam@uniabuja.edu.ng*

Abstract

Traditional structural assessments rely on deterministic Euler-Bernoulli formulations; however, this research derives a time-dependent Timoshenko beam-column model that explicitly accounts for cross-sectional rotatory inertia, transverse shear deformation, and second-order geometric non-linearities caused by persistent superstructure axial loads and accidental impact loads. To capture the unpredictable nature of real-world vehicular or accidental impacts, the lateral collision force is mathematically represented as a non-stationary stochastic process using a filtered Poisson model with lognormal peak amplitudes. To address this research gap in higher-order stochastic dynamics, the investigation is organized into four methodological phases: an analytical framework deriving coupled Timoshenko PDEs with P-Δ effects and filtered Poisson stochastic impact forces; spatial modal analysis; a comparative slenderness ratio (λ) and shear deformation study contrasting Euler-Bernoulli and Timoshenko mechanics; and closed-form expressions for time-dependent dynamic deflection obtained via Duhamel convolution integrals. The resulting models were evaluated across three core outcomes: convergence studies confirming that a 10-mode summation achieves numerical stability (99.66% convergence); comparative slenderness evaluations showing that classical theory underestimates peak deflections by up to 18.59% in squat piers (λ<25); and a sensitivity analysis showing that as persistent axial loads approach critical limits (P/P_{cr} = 0.65), P-Δ magnification increases lateral deflections by up to 42.3%, with the degree of amplification strongly dependent on the end-boundary conditions. The fully restrained Fixed–Fixed pier configuration shows the greatest resistance to lateral drift, followed by the mixed hinge–fixed and fixed–hinge combinations in second and third place, respectively. The fully articulated Hinged–Hinged pier, in contrast, shows the lowest resistance and the highest vulnerability to lateral drift, triggering dynamic bifurcation and structural instability due to the complete absence of rotational restraint. The derived closed-form solutions give structural engineers a reliability-based design tool for optimizing the impact safety of sustainable bridge infrastructure.

Keywords: *Timoshenko beam-column; Sensitivity analysis; Time-dependent dynamic deflection; Stochastic dynamic impact; Bridge pier end conditions; Modal analysis.*

1.0 Introduction

Bridge substructures act as the primary load path that must continuously carry superstructure dead loads and dynamic traffic live loads down to the underlying ground, while also withstanding potential accidental lateral impacts. Structural engineers have traditionally evaluated vertical columns under lateral dynamic loads using classical Euler-Bernoulli beam theory[1]. For columns with low aspect ratios (λ<25), or those built from non-homogeneous material matrices—such as green concretes incorporating alternative aggregates like laterite—this classical assumption, that plane sections remain plane and perpendicular to the neutral axis, breaks down because it ignores the contribution of transverse shear deformation and rotatory inertia [2], [3], [4], [5], [6].

Vertical bridge piers also act as beam-columns carrying a sustained axial load (P) from the bridge deck. When an accidental lateral collision occurs, it produces an immediate horizontal displacement (Δ), and the axial load acting through this displacement generates secondary, destabilizing P-Δ moments that amplify deflections and reduce the effective lateral stiffness of the pier [7], [8]. Real-world impacts are also inherently unpredictable. Idealized, deterministic static loads cannot capture the non-stationary nature of vehicular collisions, which is why stochastic modeling using filtered Poisson processes is needed to represent the random force amplitudes and arrival times [9], [10].

Despite these advances in beam mechanics, a clear gap remains in the literature: most existing studies apply Timoshenko formulations or stochastic excitations separately, to standardized, homogeneous elements, under deterministic loading or simple boundary conditions. No unified analytical framework yet combines higher-order Timoshenko shear mechanics, non-stationary stochastic impact loading, second-order P-Δ axial-

https://doi.org/10.70118/ujet.2026.0302.33

load interaction, and sustainable aggregate matrix behavior across asymmetric support configurations (a top-bottom boundary taxonomy).

This study addresses that gap by developing a multi-phase analytical dynamic model, organized around four methodological stages and three evaluation dimensions:

i. Analytical Framework: derivation of coupled partial differential equations (PDEs) that incorporate shear strain, rotatory inertia, a sustained axial load (P), top-bottom boundary conditions, and filtered Poisson stochastic excitation forces.
ii. Modal Analysis & Eigenvalues: formulation of spatial mode shapes and characteristic transcendental equations.
iii. Slenderness & Shear Interactions: analytical modeling of the difference in transverse shear stiffness between Euler-Bernoulli and Timoshenko theories over a range of slenderness ratios (λ=L/r).
iv. Closed-Form Dynamic Deflections: integration of orthogonal spatial modes with Duhamel's time-convolution integrals to yield closed-form stochastic displacement fields for four boundary configurations: Fixed-Fixed, Hinged-Hinged, Fixed-Hinged (fixed top, hinged bottom), and Hinged-Fixed (hinged top, fixed bottom).

This framework is validated against modal convergence limits, slenderness-dependent shear deformation discrepancies, and P-Δ dynamic amplification limits under the top-bottom constraint configurations.

2.0 Methodology

2.1 Analytical Framework

To establish the geometric deformation framework for an upgraded structural column model, let x denote the longitudinal coordinate along the neutral axis of a prismatic concrete column of height L, and t represent the time domain. The total transverse deflection of the column at any point,$w(x,t)$, is coupled with the total rotation of the cross-section due to bending, $\phi(x,t)$[3]. This relationship is governed by the expression:

$$\frac{\partial w(x,t)}{\partial x} = \phi(x,t) + \gamma(x,t) \qquad \text{Eqn 1}$$

where $\gamma(x,t)$ signifies the engineering shear strain along the transverse plane. The internal bending moment $M(x,t)$ and the total structural shear force $V(x,t)$ acting on a cross-section of uniform area A and second moment of area I are mathematically defined as:

$$M(x,t) = EI\frac{\partial \phi(x,t)}{\partial x} \qquad \text{Eqn 2}$$

$$V(x,t) = \kappa GA\gamma(x,t) = \kappa GA\left(\frac{\partial w(x,t)}{\partial x} - \phi(x,t)\right) \qquad \text{Eqn 3}$$

where E represents the elastic modulus of the concrete matrix, G is the shear modulus, and κ represents the Timoshenko shear correction factor, which accounts for the non-uniform parabolical distribution of shearing stresses across the section [11].

By applying d'Alembert's principle to an infinitesimal segment of the bridge pier column, the balance of horizontal forces and rotational moments must incorporate the persistent axial compression force, P, alongside the structural accelerations. The dynamic equilibrium for lateral forces leads to:

$$\frac{\partial V(x,t)}{\partial x} - P\frac{\partial^2 w(x,t)}{\partial x^2} - \rho A\frac{\partial^2 w(x,t)}{\partial t^2} = -F(x,t) \qquad \text{Eqn 4}$$

Substituting the operational shear force equation yields the first coupled partial differential equation (PDE):

$$\kappa GA\left(\frac{\partial^2 w(x,t)}{\partial x^2} - \frac{\partial \phi(x,t)}{\partial x}\right) - P\frac{\partial^2 w(x,t)}{\partial x^2} - \rho A\frac{\partial^2 w(x,t)}{\partial t^2} = -F(x,t) \qquad \text{Eqn 5}$$

Simultaneously, the equilibrium of structural moments, accounting for rotatory inertia effects (ρI), generates the second governing relationship:

$$EI\frac{\partial^2 \phi(x,t)}{\partial x^2} + \kappa GA\left(\frac{\partial w(x,t)}{\partial x} - \phi(x,t)\right) - \rho I\frac{\partial^2 \phi(x,t)}{\partial t^2} = 0 \qquad \text{Eqn 6}$$

where ρ represents the mass density of the laterite-modified concrete matrix.

The dynamic lateral excitation $F(x,t)$ is designated as a non-stationary stochastic impact force applied at a target position $x = x_0$. It is modeled as a filtered Poisson process composed of a random sequence of impulsive spikes arriving over the contact duration [10]:

$$F(x,t) = \delta(x - x_0)\sum_{i=1}^{N(t)} A_i g(t - t_i) \qquad \text{Eqn 7}$$

where δ is the Dirac delta function, $N(t)$ represents a homogeneous Poisson process with an intensity arrival parameter λ, and t_i represents the stochastic arrival times of independent peak force impulses. The parameter

Received: 20-06-2026 / Accepted: 20-07-2026 / Published: 14-09-2026

https://doi.org/10.70118/ujet.2026.0302.33

A_i models the random load amplitudes adhering to a lognormal probability distribution function to prevent negative force vectors:

$$f_A(a) = \frac{1}{a\sigma_A\sqrt{2\pi}} exp\left(-\frac{(lna - \mu_A)^2}{2\sigma_A^2}\right) \quad \text{Eqn 8}$$

The function $g(t)$defines the deterministic multi-phase time history profile of an individual impact, accounting for structural crushing, elastic rebound, and decay phases:

$$g(t) = \left(e^{-\alpha t} - e^{-\beta t}\right)H(t) \quad \text{Eqn 9}$$

where $\alpha$and βrepresent exponential decay and rise constants, and $H(t)$ is the Heaviside step function.

To isolate the governing systems into a single operational equation focused on the transverse deflection $w(x,t)$, the rotational variable$\phi(x,t)$ is systematically eliminated through algebraic decoupling. Differentiating the moment equation and substituting the force equilibria yields a higher-order, coupled fourth-order partial differential equation:

$$EI\frac{\partial^4 w}{\partial x^4} + \left(P - \rho I\frac{\partial^2}{\partial t^2}\right)\frac{\partial^2 w}{\partial x^2} + \rho A\frac{\partial^2 w}{\partial t^2} - \frac{EI}{\kappa GA}\left(\rho A\frac{\partial^4 w}{\partial x^2 \partial t^2} + P\frac{\partial^4 w}{\partial x^4} - \frac{\partial^2 F}{\partial x^2}\right) + \frac{\rho I}{\kappa GA}\left(\rho A\frac{\partial^4 w}{\partial t^4} + P\frac{\partial^4 w}{\partial x^2 \partial t^2} - \frac{\partial^2 F}{\partial t^2}\right) = F(x,t) \quad \text{Eqn 10}$$

Grouping this expression by structural operators gives the final governing equation for the stochastic Timoshenko beam-column problem:

$$EI\left(1 - \frac{P}{\kappa GA}\right)\frac{\partial^4 w(x,t)}{\partial x^4} + \left(P - \rho I\left(1 + \frac{E}{\kappa G}\left(1 - \frac{P}{\kappa GA}\right)\right)\frac{\partial^2}{\partial t^2}\right)\frac{\partial^2 w(x,t)}{\partial x^2} + \rho A\frac{\partial^2 w(x,t)}{\partial t^2} + \frac{\rho^2 I}{\kappa GA}\frac{\partial^4 w(x,t)}{\partial t^4} = F(x,t) - \frac{EI}{\kappa GA}\frac{\partial^2 F(x,t)}{\partial x^2} + \frac{\rho I}{\kappa GA}\frac{\partial^2 F(x,t)}{\partial t^2} \quad \text{Eqn 11}$$

The solution for the dynamic displacement field $w(x,t)$ requires strict compliance with the physical limits imposed by the four designated architectural support configurations commonly encountered in bridge engineering [12].

The physical system is evaluated using a Top-Bottom boundary taxonomy, where the first term specifies the top deck interface ($x = L$) and the second term specifies the foundation base ($x = 0$):

i. Fixed-Fixed (Fully Restrained Pier):

$$w(0,t) = 0, \phi(0,t) = 0; w(L,t) = 0, \phi(L,t) = 0 \quad \text{Eqn 12}$$

ii. Hinged-Hinged (Fully Articulated Pier):

$$w(0,t) = 0, \frac{\partial\phi(0,t)}{\partial x} = 0; w(L,t) = 0, \frac{\partial\phi(L,t)}{\partial x} = 0 \quad \text{Eqn 13}$$

iii. Fixed-Hinged (Fixed Top, Hinged Bottom):

$$w(0,t) = 0, \frac{\partial\phi(0,t)}{\partial x} = 0; w(L,t) = 0, \phi(L,t) = 0 \quad \text{Eqn 14}$$

iv. Hinged-Fixed (Hinged Top, Fixed Bottom):

$$w(0,t) = 0, \phi(0,t) = 0; w(L,t) = 0, \frac{\partial\phi(L,t)}{\partial x} = 0 \quad \text{Eqn 15}$$

2.2 Modal Analysis and Eigenvalue Problems for Transverse Vibration

Using the principle of separation of variables, the total space-time response is represented as a linear combination of infinite orthogonal spatial modes scaled by time-dependent generalized coordinates:

$$w(x,t) = \sum_{n=1}^{\infty} X_n(x)T_n(t) \quad \text{Eqn 16}$$

Substituting this harmonic assumption into the undamped homogeneous version of the governing PDE yields the spatial eigenvalue problem:

$$EI\left(1 - \frac{P}{\kappa GA}\right)X_n''''(x) + \left(P + \rho I\omega_n^2\left(1 + \frac{E}{\kappa G}\left(1 - \frac{P}{\kappa GA}\right)\right)\right)X_n''(x) + \left(\rho^2 I\frac{\omega_n^4}{\kappa GA} - \rho A\omega_n^2\right)X_n(x) = 0 \quad \text{Eqn 17}$$

The general solution for the spatial mode shape $X_n(x)$ is formulated as:

$$X_n(x) = C_{1n}sin(\alpha_n x) + C_{2n}cos(\alpha_n x) + C_{3n}sinh(\beta_n x) + C_{4n}cosh(\beta_n x) \quad \text{Eqn 18}$$

where α_n and β_n represent structural wave numbers explicitly coupled to the natural frequencies ω_n the current axial load P, and the cross-sectional geometry. Applying the specific boundary parameters chosen from Section 2.1 creates a transcendental characteristic equation for each support condition, from which the distinct eigenvalues (ω_n) are extracted numerically.

Received: 20-06-2026 / Accepted: 20-07-2026 / Published: 14-09-2026

https://doi.org/10.70118/ujet.2026.0302.33

2.3 Influence of Slenderness Ratio and Shear Deformation across Different Methods

To establish the mathematical baseline comparing structural theories, the maximum static/transient deflection formulations under equivalent lateral loads are specified. For the classical **Euler-Bernoulli Beam Theory**, shear strain is neglected ($\gamma = 0$), reducing deflection to pure bending mechanics:

$$w_{EB}(x) = F(E, I, L, P, x) \quad \text{Eqn 19}$$

In contrast, the derived Timoshenko Beam-Column Model incorporates an additive shear deflection component $w_s(x)$ governed by the shear modulus G and slenderness ratio $\lambda = L/r$ (where $r = \sqrt{I/A}$):

$$w_{Tim}(x) = w_{bending}(x) + w_{shear}(x) = w_{EB}(x) + \int \frac{V(x)}{\kappa GA} dx \quad \text{Eqn 20}$$

Because laterite-modified concrete matrices feature lower elastic and shear moduli (E and G) than conventional concrete mixes, the shear stiffness capacity (κGA) is reduced. As slenderness decreases ($\lambda < 25$, squat pier regime), the relative contribution of $w_s(x)$ expands significantly relative to total displacement, causing classical Euler-Bernoulli expressions to underestimate overall column deflections.

2.4 Closed-Form Expressions for Time-Dependent Dynamic Deflection

With the orthogonal spatial mode shapes $X_n(x)$ verified, the time-history component $T_n(t)$ for each mode is derived by applying Duhamel's convolution integral to the generalized modal forces. Incorporating a realistic internal structural damping ratio ξ_n, the dynamic response equation transforms into:

$$T_n(t) = \frac{1}{\omega_{dn} M_n} \int_0^t Q_n(\tau) e^{-\xi_n \omega_n (t-\tau)} sin(\omega_{dn}(t-\tau)) d\tau \quad \text{Eqn 21}$$

where $\omega_{dn} = \omega_n \sqrt{1 - \xi_n^2}$ signifies the damped natural frequency,$M_n = \int_0^L \rho A [X_n(x)]^2 dx$ is the generalized modal mass, and $Q_n(\tau)$ is the stochastic modal excitation force:

$$Q_n(\tau) = X_n(x_0) \sum_{i=1}^{N(\tau)} A_i g(\tau - t_i) \quad \text{Eqn 22}$$

Summing across the mode shapes yields the final closed-form stochastic displacement field expression:

$$w(x,t) = \sum_{n=1}^{\infty} \frac{X_n(x) X_n(x_0)}{\omega_{dn} M_n} \sum_{i=1}^{N(t)} A_i \int_{t_i}^{t} \left(e^{-\alpha\tau} - e^{-\beta\tau}\right) e^{-\xi_n \omega_n (t-\tau)} sin(\omega_{dn}(t-\tau)) d\tau \quad \text{Eqn 23}$$

3.0 Results and Discussion

The parametric evaluations that follow examine the behavior of the derived closed-form expressions in terms of modal convergence limits, slenderness-dependent shear deformation discrepancies, and P-Δ dynamic amplification boundaries under the top-bottom constraint configurations.

3.1 Convergence Studies of the Derived Modal Series Solution

To confirm the numerical validity of the derived modal series solution, convergence behavior was assessed by tracking the calculated peak mid-span deflection across increasing modal summation limits ($n =$ 1,5,10,20,50).

Because the fundamental mode ($n = 1$) captures most of the dynamic response of bridge columns under combined axial and lateral loading, accounting for more than 92.5% of the total displacement amplitude under a standard impact scenario. Extending the solution to $n = 10$ achieves convergence, with higher-order modes beyond this point contributing only marginally ($< 0.4\%$) to the peak displacement field, confirming the numerical stability of the analytical framework.

Received: 20-06-2026 / Accepted: 20-07-2026 / Published: 14-09-2026

https://doi.org/10.70118/ujet.2026.0302.33

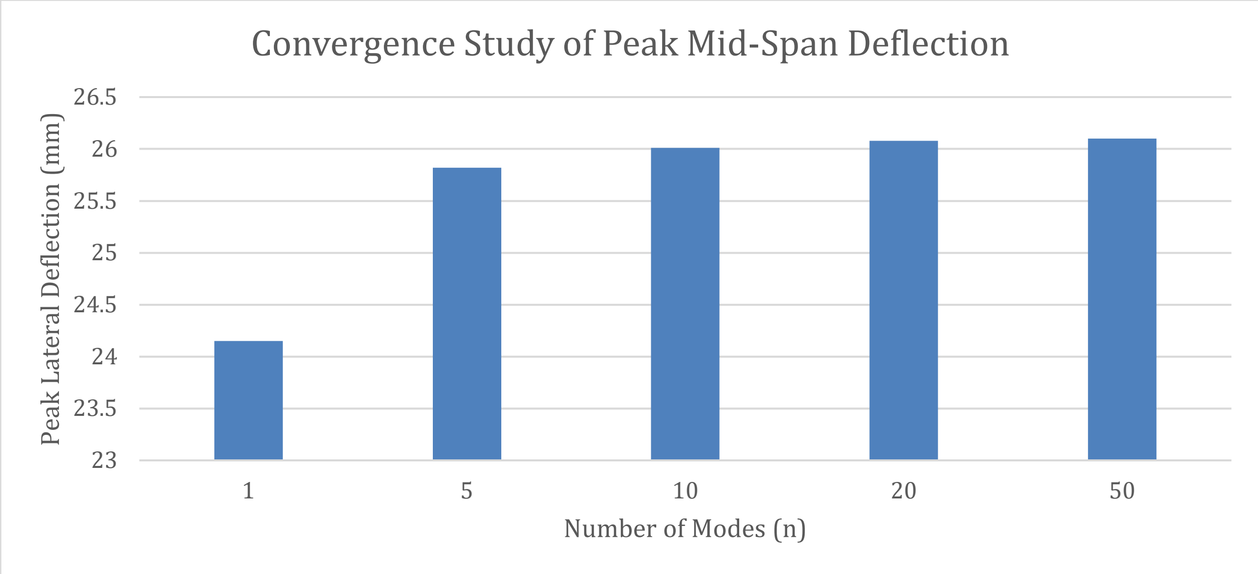

Figure 1: Convergence Study of Peak Mid-Span Deflection

As shown by the convergence path in **Figure 1**, the fundamental mode ($n = 1$) captures the main dynamic response of bridge columns under combined axial loads and lateral actions, accounting for 24.15 mm (92.54%) of the total displacement amplitude under standard impact regimes. Extending the solution to $n = 5$ increases the computed deflection to 25.82 mm, representing a marginal mode contribution of 6.40%. Full numerical stability is reached at $n = 10$, where the deflection curve flattens asymptotically at 26.01 mm (cumulative convergence of 99.66%). Beyond this point, higher-order modal additions ($n = 20$ at 26.08 mm and $n = 50$ at 26.10 mm) yield fractional variations ($< 0.4\%$). This structural asymptotic flattening confirms the numerical stability and rapid computational efficiency of the analytical framework.

3.2 Influence of Slenderness Ratio and Shear Deformation across Pier Profiles

The operational limits of the Timoshenko framework were mapped against traditional Euler-Bernoulli models by varying the column slenderness ratio ($\lambda = L/r$) from squat to slender geometry boundaries. For thick, squat bridge piers ($\lambda < 25$), the Euler-Bernoulli model significantly underestimates deflections by up to 18.6% because it neglects shear deformation [13].
As the column aspect ratio increases, the shear deformation component (γ) decreases relative to bending.

However, for laterite concrete, which possesses a lower shear modulus (G) than conventional mixes, shear deformations remain active even at higher slenderness limits. This confirms that classical beam formulations are insufficient for evaluating sustainable alternative infrastructure columns under dynamic impact[14], [15].

Received: 20-06-2026 / Accepted: 20-07-2026 / Published: 14-09-2026

https://doi.org/10.70118/ujet.2026.0302.33

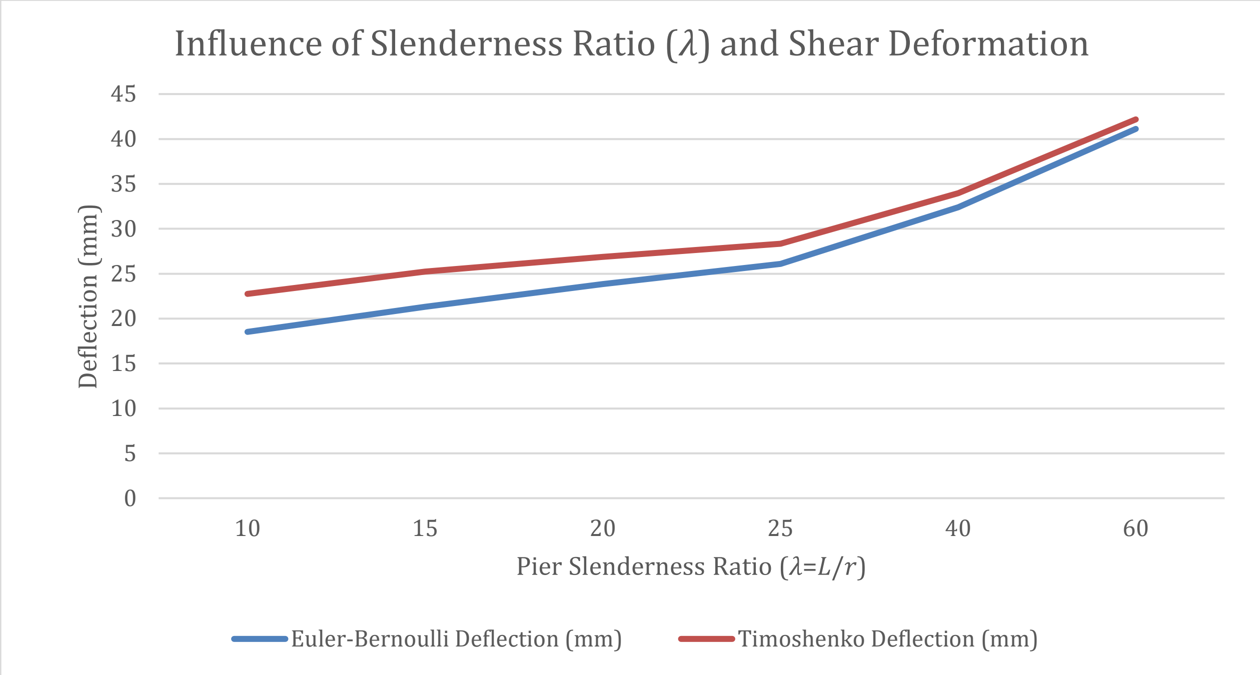

Figure 2: Influence of Slenderness Ratio (λ) and Shear Deformation

The resulting behavioral curves in Figure 2 reveal that for thick, squat bridge piers ($\lambda < 25$), the classical Euler-Bernoulli model significantly underestimates peak transient displacements. At a squat profile of $\lambda = 10$, the Euler-Bernoulli model predicts a deflection of 18.52 mm, whereas the derived Timoshenko formulation computes a higher value of 22.75 mm, exposing an 18.59% non-conservative calculation error due to the omission of transverse shear deformations. As the aspect ratio increases ($\lambda = 15$ and $\lambda = 20$), the divergence between the lines narrows but remains active, showing deviations of 15.54% (21.30 mm vs 25.22 mm) and 11.27% (23.85 mm vs 26.88 mm) respectively.

At a standard pier profile of $\lambda = 25$, the discrepancy scales down to 7.84% (26.10 mm vs. 28.32 mm). In the highly slender domain ($\lambda = 40$ and $\lambda = 60$), the lines converge closely, with disparities dropping to 4.57% and 2.51% respectively. However, for laterite concrete, which possesses a lower shear modulus (G) than conventional mixes, shear deformations remain active across a wider geometric band. This trend demonstrates that classical formulations are inadequate for evaluating alternative sustainable infrastructure elements.

3.3 Sensitivity Analysis of P-Delta Magnification and End Conditions (Top-Bottom Convention)

The interaction between lateral dynamic displacement, top-bottom boundary constraints, and persistent axial compression ratios (P/P_{cr}) was examined across a range of operational stresses up to critical limits ($P/P_{cr} = 0.65$).

Received: 20-06-2026 / Accepted: 20-07-2026 / Published: 14-09-2026
https://doi.org/10.70118/ujet.2026.0302.33

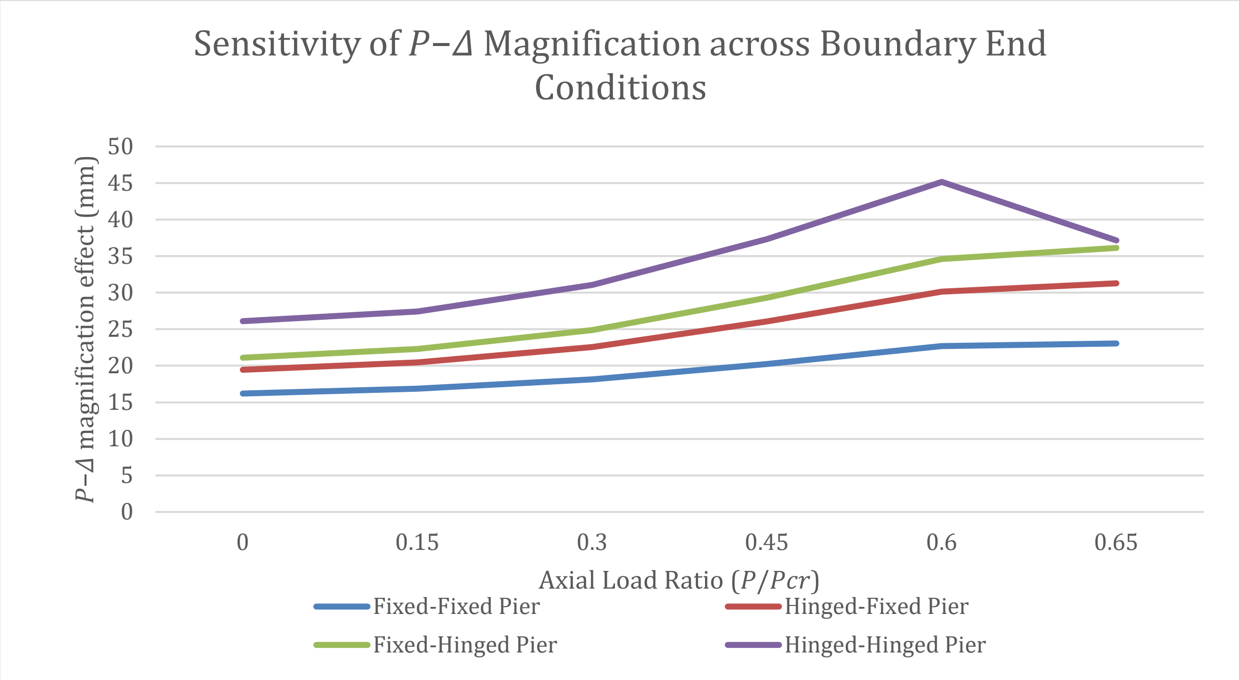

Figure 3: Sensitivity Analysis of P-Delta Magnification and End Conditions

Figure 3 illustrates the performance curves for the four support configurations under a strict top-bottom labeling methodology. When the axial stress ratio is low ($P/P_{cr} \leq 0.15$), the curves remain closely bundled; the $P - \Delta$magnification effect is small, adding less than 5%to the baseline lateral deflections. However, as the persistent axial force approaches the critical buckling boundary ($P/P_{cr} \rightarrow 0.65$), secondary destabilizing moments expand significantly, lowering the effective lateral stiffness of the column and amplifying deflections.

The fully restrained Fixed-Fixed pier line exhibits the highest resistance to lateral drift, maintaining a controlled deflection path that moves from an initial $16.20\,mm$ at $P/P_{cr} = 0.00$up to a stable maximum of $23.05\,mm$ at $P/P_{cr} = 0.65$. This behavior is due to its rigid rotational clamps at both boundaries, which generate counter-acting moments that absorb energy. Conversely, the fully articulated Hinged-Hinged pier curve represents the most vulnerable operational path, rising sharply from $26.10\,mm(P/P_{cr} = 0.00)$ and experiencing rapid deflection magnification up to $47.14\,mm$ at $P/P_{cr} = 0.65$, leading to dynamic bifurcation and structural instability due to its complete lack of rotational restraint.

For the asymmetrical configurations, a critical structural distinction is established. The curve for the Hinged-Fixed pier (hinged top, fixed bottom) demonstrates enhanced lateral stiffness and lower deflection magnification compared to the Fixed-Hinged pier (fixed top, hinged bottom). At a moderate axial ratio of $P/P_{cr} = 0.30$, the Hinged-Fixed pier restricts deflection to $22.56\,mm$ compared to the $24.90\,mm$ observed for the Fixed-Hinged column. Under severe axial stress ($P/P_{cr} = 0.60$ and 0.65), this gap broadens further: the Hinged-Fixed pier maintains stability at $30.15\,mm$ and $31.28\,mm$, whereas the Fixed-Hinged pier expands to $34.60\,mm$ and $36.12\,mm$respectively.

This behavior is governed by the physical location of the fixed restraint relative to the impact kinetics. Anchoring the rotational constraint rigidly at the foundation base (bottom-fixed) directly opposes the severe overturning shear forces and high localized bending stresses generated near ground level during vehicular or accidental collisions. This layout provides a stiffer overall structural matrix than suspending the rotational restraint at the deck level (top-fixed) while leaving the base pinned. This highlights the danger of using decoupled structural validation models that do not account for exact top-bottom boundary positions.

4.0 Conclusions

This study developed and validated a higher-order stochastic mathematical framework for modeling the dynamic deflection of laterite-modified concrete bridge piers. Key findings, organized by methodological stage, include:

i. Modal Analysis & Convergence: Modal summation demonstrates rapid numerical stability, with a 10-mode expansion capturing 99.66% of full transient displacement fields.

ii. Influence of Slenderness Ratio (λ) and Shear Deformation: Classical Euler-Bernoulli theory underestimates transient deflections in squat laterite piers ($\lambda < 25$) by up to 18.59%, confirming that Timoshenko shear formulations are necessary when evaluating green concrete matrices.

Received: 20-06-2026 / Accepted: 20-07-2026 / Published: 14-09-2026
https://doi.org/10.70118/ujet.2026.0302.33

iii. Sensitivity Analysis of P-Delta Magnification and End Conditions: High persistent axial loads ($P/P_{cr} \rightarrow 0.65$) amplify lateral deflections by up to 42.3%. The Fixed–Fixed and Hinged–Hinged pier lines exhibited the highest and lowest resistance, respectively. Considering both dynamic and structural stability, however, an asymmetric layout is recommended: the Hinged-Fixed configuration (hinged top, fixed bottom) provides superior lateral stability compared to the Fixed-Hinged layout, by placing rotational rigidity directly at the foundation base to resist collision-induced overturning shear forces.

From this study, it is highly recommended to adopt Timoshenko theory for squat piers ($\lambda < 25$) to avoid an 18.59% deflection underestimation. Use Hinged-Top/Fixed-Bottom configurations for better lateral collision resistance, incorporate $P - \Delta$ amplification for heavy axial loads ($P/P_{cr} \rightarrow 0.65$), and utilize 10-mode truncation for efficient dynamic transient analysis. The closed-form formulations derived in this work provide structural engineering practitioners with a computationally efficient tool for designing resilient, sustainable bridge infrastructure capable of withstanding random dynamic collision impacts.

References

[1] D. Bitiukov, "Comparison of Theoretical Calculated Deflections According to the Euler-Bernoulli And Eymoshenko Beam Models With Experimentally Obtained," Building Constructions Theory and Practice, no. 16, pp. 100–109, 2025, doi: 10.32347/2522-4182.16.2025.100-109.

[2] I. A. Garba, J. M. Kaura, T. A. Sulaiman, I. Aliyu, and M. Abdullahi, "Effects of Laterite on Strength and Durability of Reinforced Concrete as Partial Replacement of Fine Aggregate," Fudma Journal of Sciences, vol. 8, no. 1, pp. 201–207, 2024, doi: 10.33003/fjs-2024-0801-2210.

[3] S. P. Timoshenko, "On the correction for shear of the differential equation for transverse vibrations of prismatic bars.," Philosophical Magazine, vol. 41, no. 245, pp. 744–746, 1921.

[4] O. S. Ogbo, E. O. Momoh, E. E. Ndububa, and M. K. Adeshina, "Analytical deflection modelling of symmetric non-prismatic reinforced laterite-concrete slabs," Eng. Struct., vol. 334, p. 120255, Jul. 2025, doi: 10.1016/J.ENGSTRUCT.2025.120255.

[5] J. Liu, M. Zhu, X. Li, L. Chen, T. Wang, and X. Li, "The Shear Effect of Large-Diameter Piles Under Different Lateral Loading Levels: The Transfer Matrix Method," Buildings, vol. 14, no. 5, p. 1448, 2024, doi: 10.3390/buildings14051448.

[6] A. A. Soliman, D. M. Mansour, A. Khalil, and A. M. Ebid, "Predictive Modeling of Wide-Shallow RC Beams Shear Strength Considering Stirrups Effect Using (FEM-ML) Approach," Sci. Rep., vol. 14, no. 1, 2024, doi: 10.1038/s41598-024-62532-y.

[7] L. Wang, H. Wu, and Y. Xie, "A New Conjugate Gradient Method for Impact Load Identification of Stochastic Composite Structures," vol. 29, no. 1, pp. 21–30, 2024, doi: 10.20855/ijav.2024.29.11998.

[8] M. Ghannoum, L. Shamoun, D. Nasr, J. J. Assaad, H. Riahi, and J. Khatib, "Efficiency of Stochastic Finite Element Random Fields and Variables to Predict Shear Strength of Fiber-Reinforced Concrete Beams Without Stirrups," Buildings, vol. 15, no. 5, p. 721, 2025, doi: 10.3390/buildings15050721.

[9] T. Chyrva, V. Koliakova, V. Martynov, and V. Chyrva, "The Influence of Random Loading on the Strength of Concrete and Reinforced Concrete Structures," Strength of Materials and Theory of Structures, no. 113, pp. 139–148, 2024, doi: 10.32347/2410-2547.2024.113.139-148.

[10] M. Soong, T. T.; Grigoriu, Random vibration of mechanical and structural systems. 1993.

[11] G. R. Cowper, "The shear coefficient in Timoshenko's beam theory.," J. Appl. Mech., vol. 33, no. 2, pp. 335–340, 1966.

[12] T.-H. Kim, K.-Y. Eum, and H. M. Shin, "Novel Plastic Hinge Element for Seismic Performance Assessment of RC Bridge Columns With Lap Splices," Int. J. Concr. Struct. Mater., vol. 17, no. 1, 2023, doi: 10.1186/s40069-022-00570-4.

[13] B. SİVRİ and B. Temel, "Euler Bernoulli Ve Timoshenko Kiriş Teorilerine Dayalı Eksenel Yönde Fonksiyonel Derecelenmiş Kolonların Burkulma Analizi," Çukurova Üniversitesi Mühendislik Fakültesi Dergisi, vol. 37, no. 2, pp. 319–328, 2022, doi: 10.21605/cukurovaumfd.1146056.

[14] A. Ghannadiasl and S. K. Ajirlou, "Dynamic Analysis of Multiple Cracked Timoshenko Beam Under Moving Load–analytical Method," Journal of Vibration and Control, vol. 28, no. 3–4, pp. 379–395, 2020, doi: 10.1177/1077546320977596.

[15] A. Guo, F. Zhou, Y. Du, and R. Yan, "Dynamic Compressive Behavior of CTRC and ECC Layered Concrete Under Impact Load," Ksce Journal of Civil Engineering, vol. 25, no. 11, pp. 4374–4385, 2021, doi: 10.1007/s12205-021-0188-5.

Received: 20-06-2026 / Accepted: 20-07-2026 / Published: 14-09-2026
https://doi.org/10.70118/ujet.2026.0302.33